© 2017. Published by The Company of Biologists Ltd | Journal of Cell Science (2017) 130, 1486-1493 doi:10.1242/jcs.199968

RESEARCH ARTICLE

Oxidative stress elicited by modifying the ceramide acyl chain length reduces the rate of clathrin-mediated endocytosis

Giora Volpert[1], Shifra Ben-Dor[2], Ohad Tarcic[3], Jingjing Duan[4], Ann Saada[5,6], Alfred H. Merrill, Jr[4], Yael Pewzner-Jung[1] and Anthony H. Futerman[1,*]

ABSTRACT

Sphingolipids modulate clathrin-mediated endocytosis (CME) by altering the biophysical properties of membranes. We now examine CME in astrocytes cultured from ceramide synthase 2 (CerS2) null mice, which have an altered sphingolipid acyl chain composition. The rate of endocytosis of low-density lipoprotein and transferrin, which are internalized via CME, was reduced in CerS2 null astrocytes, although the rate of caveolin-mediated endocytosis was unaltered. Levels of clathrin heavy chain were increased, which was due to decreased levels of Hsc70 (also known as HSPA8), a protein involved in clathrin uncoating. Hsc70 levels were decreased because of lower levels of binding of Sp1 to position −68 in the Hsc70 promoter. Levels of Sp1 were downregulated due to oxidative stress, which was elevated fourfold in CerS2 null astrocytes. Furthermore, induction of oxidative stress in wild-type astrocytes decreased the rate of CME, whereas amelioration of oxidative stress in CerS2 null astrocytes reversed the decrease. Our data are consistent with the notion that sphingolipids not only change membrane biophysical properties but also that changes in their composition can result in downstream effects that indirectly impinge upon a number of cellular pathways, such as CME.

KEY WORDS: Very long-chain ceramides, Clathrin-mediated endocytosis, Reactive oxygen species, Sp1, Hsc70

INTRODUCTION

The lipid composition of the plasma membrane plays a vital role in regulating clathrin-mediated endocytosis (CME) (Lauwers et al., 2016), and sphingolipids (SLs) are of particular importance in this regard (Cheng et al., 2006). It is perhaps not surprising that SLs play such a critical role in regulating CME since SLs have distinct biophysical properties, and together with cholesterol, ceramide and sphingomyelin (SM) increase the order and reduce the fluidity of membranes, leading to increased rigidity, tighter packing and formation of ceramide-enriched microdomains (Pinto et al., 2013). These microdomains enable amplification of signaling pathways by reorganizing the membrane and clustering specific signaling components (Zhang et al., 2009).

Most studies examining the role of SLs in CME have been performed using inhibitors of SL biosynthesis (Meyer et al., 2012) or by altering levels of specific SL classes, such as SM (Shakor et al., 2011). We previously demonstrated that altering the SL acyl chain length also leads to changes in membrane biophysical properties (Silva et al., 2012), which may be one of the reasons that ceramide synthase 2 (CerS2) null mice, which are unable to synthesize very long-chain SLs (Pewzner-Jung et al., 2010a,b), displays a variety of phenotypes related to ligand and receptor internalization (Ali et al., 2013; Park et al., 2012, 2014). However, mechanistic information on how CME is regulated by the SL acyl chain composition is unavailable. We now analyze CME in astrocytes that have been cultured from CerS2 null mice, and show that they contain elevated levels of reactive oxygen species (ROS), which trigger a reduction in the transcription of Hsc70 (also known as HSPA8) – a protein involved in uncoating clathrin vesicles – and as a consequence, reduces the rate of CME but not of endocytosis via caveolin-mediated pathways. We suggest that, at least in astrocytes, CME is not directly regulated by the SL acyl chain composition but rather via a downstream pathway that is modulated by the oxidative state of the cell.

RESULTS

Characterization of astrocytes from CerS2 null mice

In mammals, endocytosis of nutrients by astrocytes is important for normal neuronal function (Jiang and Chen, 2009). Astrocytes were isolated from wild-type (WT) and CerS2 null mice. The cultures contained ∼95% astrocytes and <0.1% microglia [using an antibody against glial fibrillary acidic protein (GFAP) to detect astrocytes and against CD68 to detect microglia] (Fig. 1A). As expected, in CerS2 null astrocytes, mRNA levels of CerS2 were undetectable and mRNA levels of the other five mammalian CerS proteins (Levy and Futerman, 2010) were unaltered (Fig. 1B). Likewise, CerS2 activity was undetectable in CerS2 null astrocytes using C24:1-CoA as substrate, although a small amount of residual activity could be detected using C22:0-CoA (Fig. 1C), probably due to the partial overlapping substrate specificities of CerS4 and CerS2 (Riebeling et al., 2003). Analysis of the astrocyte SL composition was consistent with mRNA and CerS-protein activity levels, in so far as C24:1-ceramide was barely detectable in CerS2 null astrocytes [as were levels of the more complex SLs, C24:1-SM and C24:1-glucosylceramide (not shown)], and C22:0-ceramide levels were reduced by ∼35% compared to those in WT astrocytes (Fig. 1D). Total ceramide levels were essentially unaltered (Fig. 1D) due to increased levels of C16:0- and

[1]Department of Biomolecular Sciences, Weizmann Institute of Science, Rehovot 76100, Israel. [2]Department of Biological Services, Weizmann Institute of Science, Rehovot 76100, Israel. [3]Department of Molecular Cell Biology, Weizmann Institute of Science, Rehovot 76100, Israel. [4]School of Biology and Petit Institute for Bioengineering and Bioscience, Georgia Institute of Technology, Atlanta, GA 30332-0230, USA. [5]Monique and Jacques Roboh Department of Genetic Research, Hadassah-Hebrew University Hospital, Jerusalem 91120, Israel. [6]The Department of Genetic and Metabolic Diseases, Hadassah-Hebrew University Hospital, Jerusalem 91120, Israel.

*Author for correspondence (tony.futerman@weizmann.ac.il)

A.H.F., 0000-0003-0013-0115

Received 21 November 2016; Accepted 28 February 2017

Journal of Cell Science (2017) 130, 1486-1493 doi:10.1242/jcs.199968

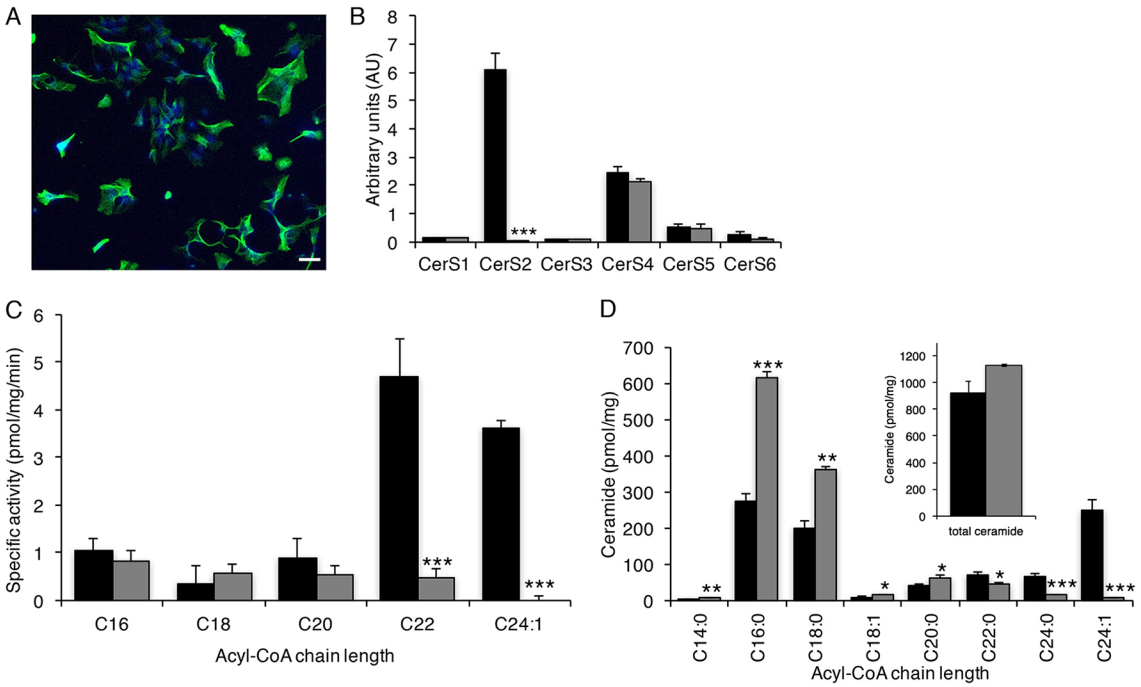

Fig. 1. Characterization of CerS2 null astrocytes. (A) Astrocytes were purified and co-stained with antibodies against GFAP (green) and CD68 (red). Nuclei were stained with Hoechst 33348 (blue). Scale bar: 40 µm. (B) mRNA levels of CerS isoforms, normalized to expression of *HPRT*. Values are means±s.e.m., $n \geq 3$. ***P<0.001 (Student's *t*-test). (C) Activity of CerS proteins using different acyl-CoAs. Values are means±s.e.m., $n \geq 4$. ***P<0.001 (Student's *t*-test). (D) Mass spectrometry analysis of ceramide species. Values are means±s.e.m., n=3 for CerS2 null, n=2 for WT. *P<0.05; **P<0.01; ***P<0.001 (Student's *t*-test). The inset shows total ceramide levels. In panels B-E, WT data is black and CerS2 null is gray.

C18:0-ceramide, similar to changes in the SL profile in CerS2 null mouse liver (Pewzner-Jung et al., 2010b). However, unlike in liver, levels of the long-chain bases – sphinganine (3.9±0.7 pmol/mg in WT and 5.6±1.1 pmol/mg in CerS2 null mice; mean±s.d.) and sphingosine (86.4±3.4 pmol/mg in WT and 75.2±3.3 pmol/mg in CerS2 null mice) – were essentially unaltered.

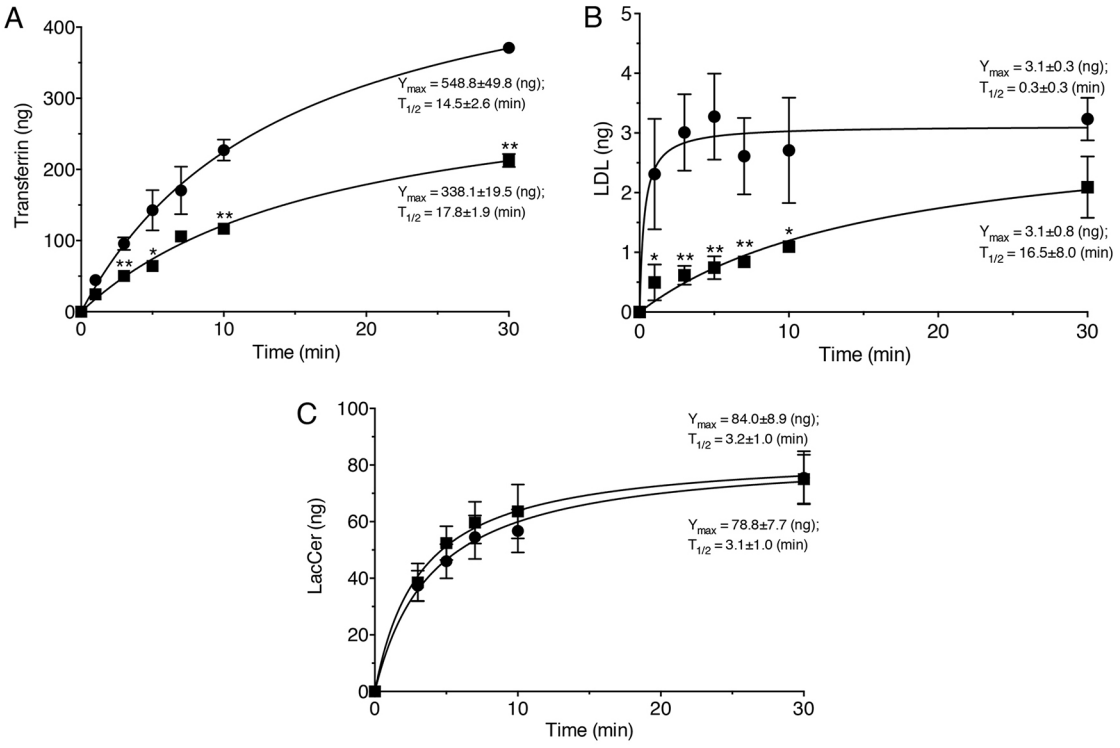

Fig. 2. The rate of CME in CerS2 null astrocytes. Cells were incubated with (A) DiI–LDL, (B) Cy5–Tf or (C) BODIPY–LacCer for various times, and the amount of internalized ligand was analyzed. Values are means±s.e.m., n=3. *P<0.05; **P<0.01 (Student's *t*-test). WT is indicated by circles and CerS2 null by squares.

Journal of Cell Science (2017) 130, 1486-1493 doi:10.1242/jcs.199968

Reduced rates of CME in astrocytes from CerS2 null mice

We next examined the rate of CME in astrocytes using two fluorescently labeled ligands (Keyel et al., 2006). Both 1,1′-dioctadecyl-3,3,3′,3′-tetramethylindocarbocyanine (Dil)-tagged low density lipoprotein (Dil–LDL) and Cy5–transferrin (Cy5–Tf) were internalized at a slower rate in CerS2 null astrocytes than in WT astrocytes (Fig. 2A,B). In contrast, the rate of caveolin-mediated endocytosis, measured using BODIPY–lactosylceramide (BODIPY–LacCer) (Singh et al., 2007), was unaltered (Fig. 2C). The differences in the kinetic parameters of uptake between Cy5–Tf (Fig. 2A) and Dil–LDL (Fig. 2B) is probably due to differences in the rate of recycling and sorting and between LDL and Tf receptors (Ghosh et al., 1994).

LDL receptor and Tf receptor levels were unchanged (Fig. 3A), suggesting that the reason for the reduced rate of CME is related to one or other aspect of CME rather than reduced levels of the receptors that bind to the ligands. Indeed, levels of the clathrin heavy chain were elevated 3.5-fold (Fig. 3A), and distinct large puncta of the clathrin heavy chain were observed in the cytoplasm of CerS2 null astrocytes (Fig. 3B), similar to that observed previously in mice that lack the clathrin-coated vesicle uncoating protein auxilin-1 (Yim et al., 2010). In the case of CerS2 null mouse astrocytes, levels of auxilin-1 mRNA were unchanged (Fig. 3C), but levels of heat shock cognate 70 (Hsc70) mRNA were reduced by ∼threefold (Fig. 3C), and protein levels were reduced by 25±5% (Fig. 3D). Hsc70 also plays a key role in the uncoating of clathrin-coated vesicles (Greene and Eisenberg, 1990).

Transcriptional regulation of Hsc70 by specificity protein 1 transcription factor

Since Hsc70 mRNA levels were reduced (Fig. 3C), we next examined the levels of two transcription factors that regulate Hsc70 expression, namely specificity protein 1 (Sp1) (Wilke et al., 2000) and heat shock factor 1 (HSF-1) (Yasuhara et al., 2011). Levels of Sp1 were reduced by 35±4% (mean±s.d.), whereas levels of HSF-1 were unaltered (Fig. 4A); the reduction in Sp1 protein levels was not due to changes in its transcription (Fig. 4B). Two putative binding motifs for Sp1 are found in positions −174 and −68 from the transcription start site of Hsc70 (Fig. 4C). Chromatin immunoprecipitation (ChIP) demonstrated that Sp1 binds to position −68, whereas no binding of Sp1 to position −174 could be detected (Fig. 4D). Sp1 binding to position −68 was significantly reduced in CerS2 null astrocytes (Fig. 4D). Levels of two other Sp1 targets, glycolipid transfer protein (Zou et al., 2011) and fatty acid synthase (Archer, 2011) were also reduced, but levels of two predicted non-targets of Sp1, GFAP and toll-like receptor 4, were unaltered (Fig. 4E). These results suggest that Hsc70 is transcriptionally regulated by Sp1 in CerS2 null astrocytes, and that additional cellular pathways regulated by Sp1 might also be affected in CerS2 null astrocytes.

CME is attenuated by the oxidative state of the cells

Sp1 is sensitive to its O-glycosylation (GlcNAc) state in so far as Sp1 hypo-glycosylation leads to its proteasomal degradation (Han and Kudlow, 1997). ROS have been shown previously to induce proteasome-mediated reduction of Sp1 levels through reduction of

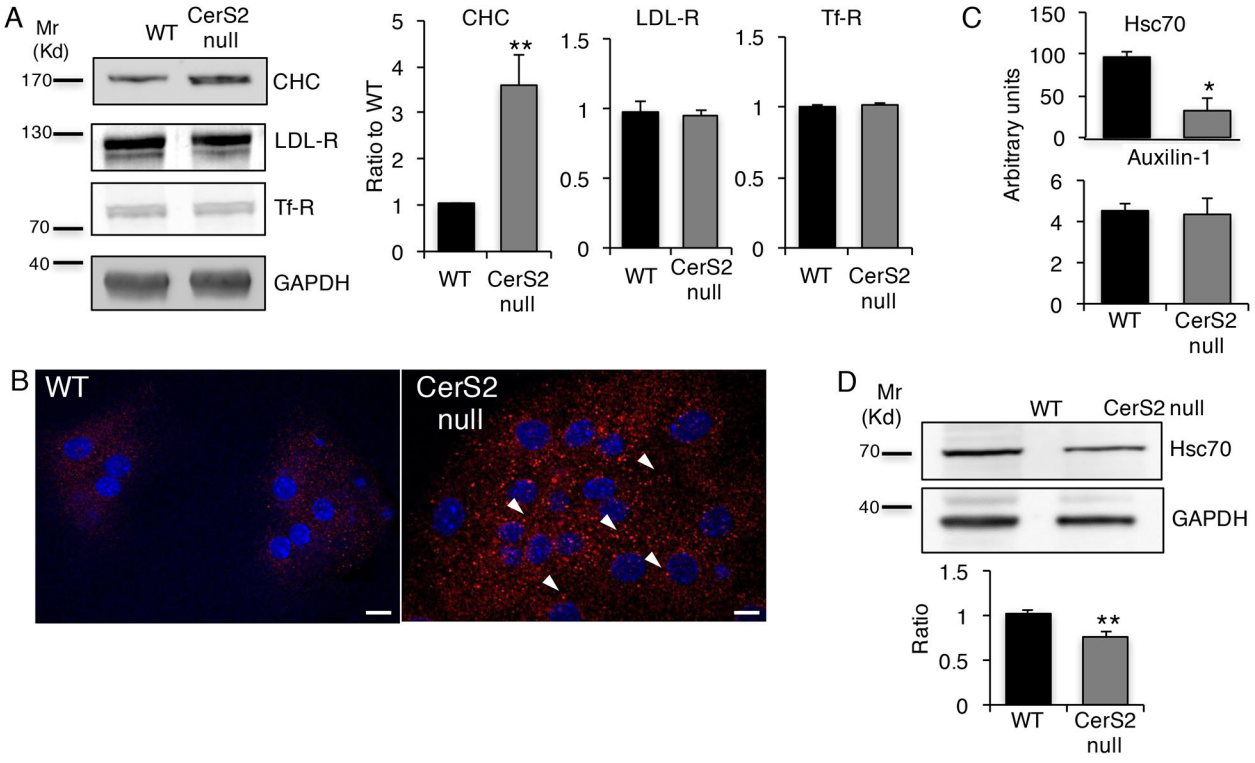

Fig. 3. Dysregulated CME in CerS2 null astrocytes. (A) Western blot of clathrin heavy chain (CHC; using a pan-CHC antibody), LDL receptor (LDL-R) and Tf receptor (Tf-R) in astrocytes. GAPDH was used as a loading control. The right-hand panel shows ratio values calculated from quantification of the western blots. Values are means±s.e.m. $^{**}P<0.01$ (Student's *t*-test). (B) Distribution of CHC determined by confocal microscopy. CHC, red; Hoechst 33348, blue. Arrowheads indicate large puncta of CHC in CerS2 null astrocytes. The images are representative of three independent experiments. Scale bars: 10 µm. (C) mRNA levels of auxilin-1 and Hsc70, normalized to expression of *TBP*. $n=2$. Values are means±s.d. $^{*}P<0.05$ (Student's *t*-test). (D) Western blot of Hsc70. GAPDH was used as a loading control. The lower panel shows ratio values calculated by quantifying the western blots. Values are means±s.e.m., $n=5$. $^{**}P<0.01$.

Journal of Cell Science (2017) 130, 1486-1493 doi:10.1242/jcs.199968

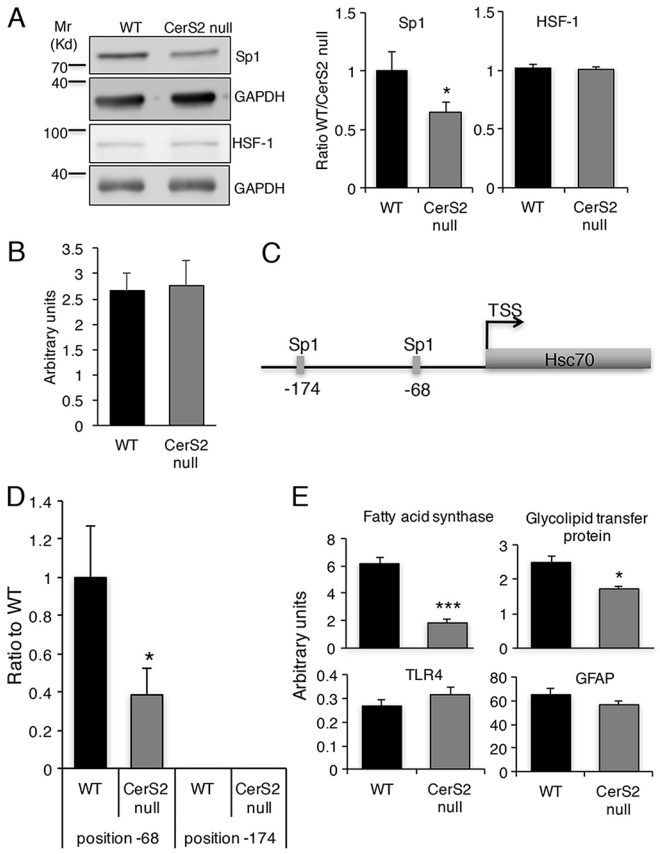

Fig. 4. Sp1 regulates Hsc70 in CerS2 null astrocytes. (A) Western blot of Sp1 and HSF-1 in WT and CerS2 null cells. GAPDH was used as a loading control. The right-hand panel shows ratio values calculated from quantification of the blots. Values are means±s.d., n=4. *P<0.05 (Student's t-test). (B) mRNA levels of Sp1, normalized to expression of *TBP*. Values are means ±s.d., n=4. (C) Schematic representation of the promoter region of the mouse Hsc70 (*Hspa8*) gene. The first exon is shown as a gray box. The transcription start site (TSS) and the two putative Sp1-binding sites are also indicated. Schematic based on mouse genome version GRCm38, chr9:40,801,066-40,801,348. (D) ChIP analysis of the binding of Sp1 transcription factor to positions −68 and −174 in the Hsc70 promoter. An antibody against HA was used as a binding control for Sp1 binding. n=3, values are means±s.e.m. *P<0.05 (Student's t-test). (E) mRNA levels of fatty acid synthase, glycolipid transfer protein, toll-like receptor 4 (TLR4) and GFAP. Values are means± s.e.m., n=3. *P<0.05; ***P<0.001 (Student's t-test).

Sp1 O-glycosylation (Kim et al., 2012), whereas N-acetyl cysteine (NAC) has been shown to mitigate this effect (Hsin et al., 2010). Thus, we next measured ROS levels in CerS2 null astrocytes, which were elevated ∼fourfold (Fig. 5A), along with a 60±18% (mean± s.d.) increase in levels of 3-nitrotyrosine (Fig. 5B). ROS overproduction in CerS2 null astrocytes is likely to be due to reduced activity of mitochondrial respiratory chain complex IV (also known as COX) (Fig. 5C), similar to that observed in the liver from CerS2 null mice (Zigdon et al., 2013). Based on these results, we suggest a pathway exists by which oxidative stress in CerS2 null astrocytes results in lower Sp1 levels and hence lower levels of Hsc70, which directly affects the rate of CME. This was tested by inducing ROS, using H_2O_2, in WT astrocytes, which resulted in a slower rate of uptake of Cy5–Tf, and by ameliorating ROS levels in CerS2 null astrocytes with NAC, which resulted in increased rates of Cy5–Tf uptake (Fig. 6A,B). Similar results were seen with Dil–LDL (Fig. 6C,D). Concomitantly, H_2O_2 treatment decreased Sp1 and Hsc70 levels in WT astrocytes to levels similar to those in untreated CerS2 null astrocytes, whereas treatment with NAC increased their levels in CerS2 null astrocytes to the same levels as in untreated WT astrocytes (Fig. 6E). Neither ROS nor NAC affected LDL receptor or Tf receptor levels in WT or CerS2 null astrocytes (Fig. 6E).

DISCUSSION

In the current study, we demonstrate a new mechanism by which altering the SL acyl chain length can affect the rate of CME, which is apparently independent of changes in membrane biophysical properties. In this pathway, oxidative stress, caused by ROS overproduction via mitochondrial complex IV dysfunction, as observed in hepatocytes upon loss of very-long acyl chain ceramides and elevation of long-chain ceramides (Zigdon et al., 2013), results in downregulation of the transcription factor Sp1, which binds to the promoter region of Hsc70, a key player involved in removing the clathrin coat. As a result, clathrin aggregates in the cytoplasm, rendering it inaccessible for additional rounds of CME (Fig. 7). Disruption of another uncoating protein, auxilin-1 (Yim et al., 2010), results in a similar phenotype, as does knockdown of Hsc70 (Yu et al., 2014), whereas a complete knockout of Hsc70 in mice is embryonically lethal (Florin et al., 2004), and auxilin-1 knockout mice exhibit elevated levels of clathrin heavy chain (Hirst et al., 2008) and reduced CME (Yim et al., 2010).

SLs can reside in lipid rafts (Simons and van Meer, 1988), platforms through which caveolae are formed and, thereby, they mediate uptake of ligands through caveolin-mediated endocytosis (Mayor and Pagano, 2007). Although we observed significant changes in the SL profile of CerS2 null astrocytes, caveolin-mediated endocytosis was unaltered, presumably since total ceramide levels were unaltered in CerS2 null astrocytes.

We have previously observed a number of changes in receptor activation and/or internalization in hepatocytes. For instance, altering the SL acyl chain composition abrogates insulin receptor phosphorylation, but this effect is directly caused by changes in membrane biophysical properties, with the insulin receptor unable to translocate into detergent-resistant membranes (Park et al., 2012). Likewise, palmitic acid is not internalized by CerS2 null hepatocytes, caused by the inability of CD36 (also known as FAT) to translocate into detergent-resistant membranes before internalization (Park et al., 2014). The mechanism by which tumor necrosis factor α receptor-1 internalization is inhibited in CerS2 null hepatocytes has not been established (Ali et al., 2013), but we have suggested that this might be related to the altered recruitment of adaptor proteins required for clathrin-coated pit formation. Finally, altering the SL acyl chain composition also affects intracellular trafficking of connexin 32 (Park et al., 2013), again due to altered biophysical properties. Thus, SLs have direct effects on receptor internalization and trafficking but also indirect effects, such as those reported in the current study, whereby dysfunction of mitochondrial complex IV affects ROS levels and results in concomitant changes in pathways affected by ROS, such as endocytosis (Parry et al., 2008; Poumay and Ronveaux-Dupal, 1988). Whether similar changes in signaling pathways occur upon acute changes in SL levels (Morales et al., 2007) is currently unknown, but the current study highlights the need to pay attention to both direct effects of SLs on membrane biophysical properties and also to indirect effects caused by activation of downstream pathways, such as defective clathrin uncoating caused by oxidative stress.

MATERIALS AND METHODS

Astrocyte cultures

Cortical astrocytes from 2- to 4-day-old WT and CerS2 null mice (Pewzner-Jung et al., 2010b) were isolated as described (Schildge et al., 2013). Astrocytes

Journal of Cell Science (2017) 130, 1486-1493 doi:10.1242/jcs.199968

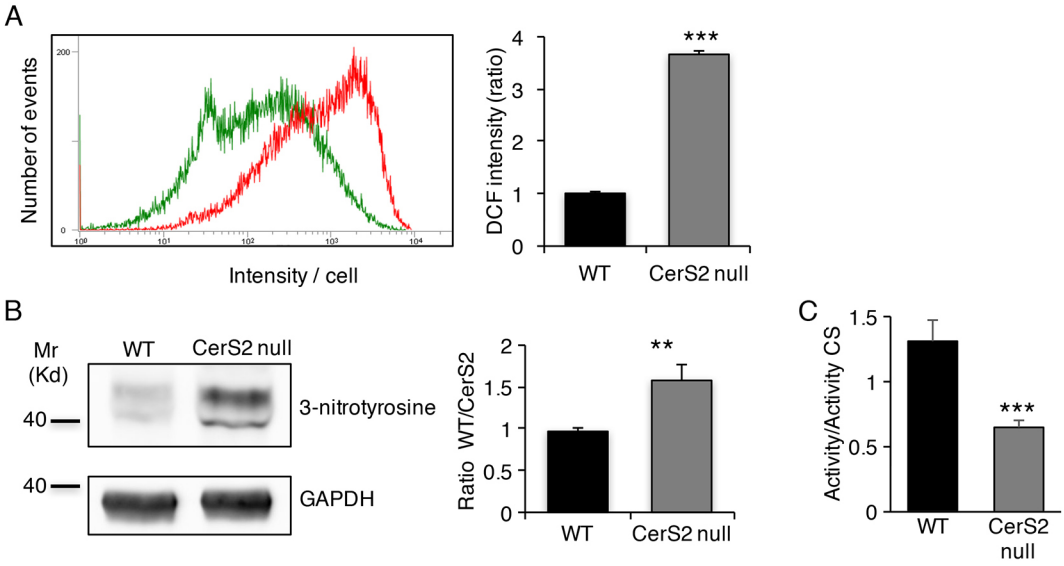

Fig. 5. Increased oxidative stress in CerS2 null astrocytes. (A) FACS analysis of ROS levels in WT (green) and CerS2 null (red) astrocytes using cmH2DCF-DA. Individual samples contained at least 30,000 cells. The right-hand panel shows quantification of ROS in CerS2 null cells relative to those in WT. n=3. Values are means±s.e.m. ***P<0.001 (Student's t-test). (B) Western blot of 3-nitrotyrosine. GAPDH was used as a loading control. The right-hand panel shows quantification. n=4. Values are means±s.d., **P<0.01 (Student's t-test). (C) Activity of mitochondrial complex IV normalized to that of citrate synthase (CS) in WT and CerS2 null astrocytes. Values are means±s.d., n=4. ***P<0.001 (Student's t-test).

were grown to 95% confluence for 7-10 days, other cells were removed from the dishes by vigorous shaking (2 h, 200 rpm on an orbital shaker), and astrocytes were replated and grown to 95% confluence for up to 23 days. Cells were cultured in Dulbecco's modified eagle's medium (DMEM, Gibco™) containing 10% fetal calf serum (Gibco™) and 2% penicillin-streptomycin.

Immunohistochemistry

Astrocytes were cultured on 12- or 13-mm glass coverslips to a confluence of ~70%. Cells were fixed by incubating with 3% paraformaldehyde in phosphate buffered saline (PBS) at room temperature for 15 min, rinsed three times with PBS for 4 min and blocked with 4% bovine serum albumin for 90 min. Cells were then either co-incubated for 1 h with anti-GFAP (for astrocytes, 1:1000; cat. no. 4560-0204, Bio-Rad) and anti-CD68 (for microglia, 1:1000; cat. no. MCA1957, Bio-Rad laboratories) antibodies, or with an anti-clathrin heavy chain (1:50; cat. no. CR796S, Cell Signaling) antibody. Cells were washed three times with PBS for 4 min and incubated with a secondary fluorescently labeled antibody (anti-rat, anti-mouse or anti rabbit; 1:250, Jackson Immunoresearch Labs) for 60 min. Cells were rinsed three times with PBS for 4 min, incubated for 10 min with Hoechst 33342 (1:5000, Molecular Probes) and then rinsed three times with PBS for 4 min. Glass coverslips were mounted on slides using Gel Mount (Molecular Probes, Eugene, Oregon, USA) and analyzed by fluorescence microscopy using an Olympus IX 81 FluoView 1000 microscope (Olympus, Tokyo, Japan).

RNA extraction and PCR

Total RNA was isolated using the RNeasy mini kit (Qiagen) according to the manufacturer's instructions. cDNA synthesis was performed using a Verso cDNA kit (Thermo Scientific). Quantitative (q)PCR was performed as described previously (Vitner et al., 2016). The relative amounts of mRNA were calculated from the cyclic threshold values using hypoxanthine guanine phosphoribosyl transferase (HPRT) or TATA binding protein (TBP) for normalization. Primers are listed in Table S1.

CerS protein assays

Cells were homogenized in 20 mM HEPES-KOH, pH 7.2, 25 mM KCl, 250 mM sucrose and 2 mM $MgCl_2$ containing a protease inhibitor cocktail (Sigma). Protein content was determined using the BCA reagent (Pierce). Homogenates were incubated with 15 µM NBD-sphinganine (Tidhar et al., 2014) (Avanti Polar Lipids), 20 µM de-fatted bovine serum albumin (Sigma) and 50 µM C16:0-CoA (for CerS5 and CerS6), C18:0-CoA (for CerS1 and CerS4), C20:0-CoA (for CerS4) and C22:0-CoA, C24:0-CoA or C24:1-CoA (for CerS2) (Avanti Polar Lipids) for 5-40 min at 37°C. Lipids were extracted and separated by performing thin layer chromatography using chloroform:methanol:2 M NH_4OH (40:10:1, v/v/v) as the developing solvent. NBD-labeled lipids were visualized using a Typhoon 9410 variable mode imager and quantified using ImageQuantTL software (GE Healthcare).

Lipid analysis

SL analysis using liquid chromatography-coupled electrospray ionization tandem mass spectrometry (LC-ESI MS/MS) was performed using a PE-Sciex API 3000 triple quadrupole mass spectrometer and an ABI 4000 quadrupole-linear ion trap mass spectrometer (Shaner et al., 2009; Sullards et al., 2011).

Uptake of fluorescently labeled ligands

WT and CerS2 null astrocytes were cultured in 96-well plates and grown overnight. Cells were incubated for various times with fluorescently labeled ligands [Dil–LDL (1:100), BODIPY–LacCer (1:100) from Life Technologies; Cy5–Tf (1:100) from Jackson Immunoresearch Labs]. Cells were washed three times with PBS to remove unbound ligand and incubated for 4 min with 500 mM NaCl in 200 mM acetic acid, pH 3.5, to remove Dil–LDL or to remove Cy5–Tf bound to the cell surface (Megias et al., 2000). For BODIPY–LacCer, 'back exchange' was performed by incubating cells with 5% de-fatted bovine serum albumin for 10 min. In some cases, cells were incubated with 100 µM H_2O_2 or 100 µM NAC for 4 h before addition of the fluorescent ligand. Internalized fluorescent ligand was quantified using a plate reader at the following wavelengths: Dil–LDL, excitation 528 nm, emission 590 nm; BODIPY-LacCer, excitation 485 nm, emission 528 nm; Cy5–transferrin, excitation 630 nm, emission 680 nm.

Western blotting

Western blotting (Zigdon et al., 2015) was performed with the following antibodies diluted in PBS and 0.1% Tween-20: rabbit pan anti-CHC (1:1000; cat. no. C4796S, Cell Signaling); rabbit pan anti-LDL receptor (1:1000, cat. no. AB30532), mouse anti-Hsc70 (1:1000, cat. no. ab2788), rabbit anti-Sp1 (1:1000, cat. no. ab13370), rabbit anti-3-nitrotyrosine

Journal of Cell Science (2017) 130, 1486-1493 doi:10.1242/jcs.199968

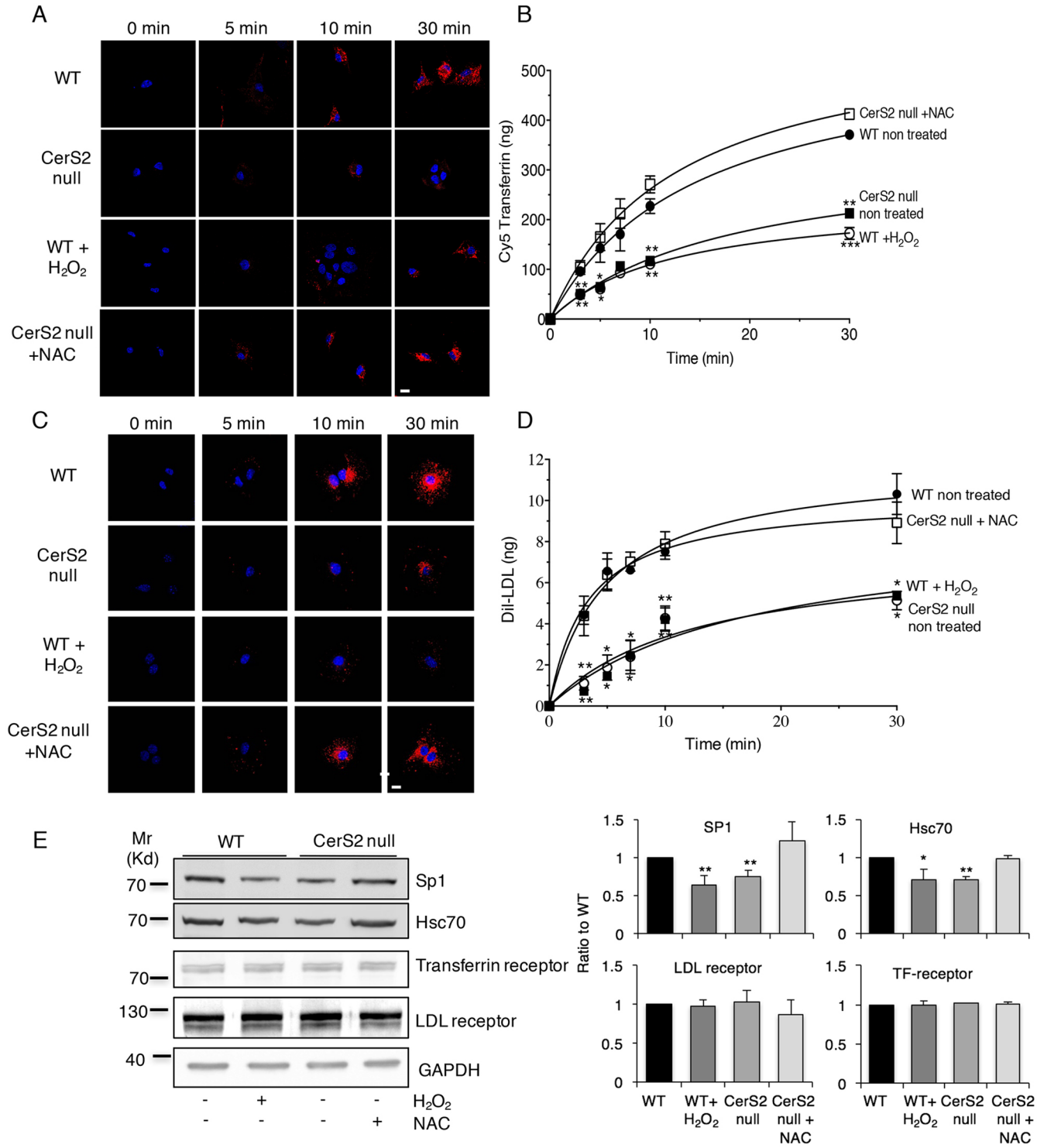

Fig. 6. Oxidative stress regulates CME through the Sp1–Hsc70 axis. Astrocytes were incubated with and without H_2O_2 (100 µM, 4 h) or NAC (100 µM, 4 h), followed by incubation with (A) Cy5–Tf (red) or (C) Dil–LDL (red) for the indicated times. Hoechst 33348, blue. Scale bars: 10 µm. Rate of uptake of (B) Cy5–Tf or (D) Dil–LDL was measured. Values are means±s.e.m., n=3. *P<0.05; **P<0.01; ***P<0.001 (Student's t-test). (E) Western blot of Sp1, Hsc70, transferrin receptor and LDL receptor. GAPDH was used as a loading control. The right-hand panel shows ratio values calculated from quantification of western blots. Values are means±s.e.m., n=3. *P<0.05; **P<0.01 (Student's t-test).

(1:1000, cat. no. ab7048) antibodies, all obtained from Abcam (Cambridge, UK); rabbit anti-Tf receptor antibody (1:1000, cat. no. sc7087, Santa Cruz); and mouse anti-GAPDH antibody (1:5000, cat. no. MAB374, Millipore). Densitometry was performed using ImageQuant software (Amersham Biosciences).

Transcription factor binding site analysis

Transcription factor binding site analysis was performed using the Genomatix Genome Analyzer (GGA) MatInspector program (Cartharius et al., 2005), Matrix Library Version 9.0, searching with the V$SP1F matrix.

Journal of Cell Science (2017) 130, 1486-1493 doi:10.1242/jcs.199968

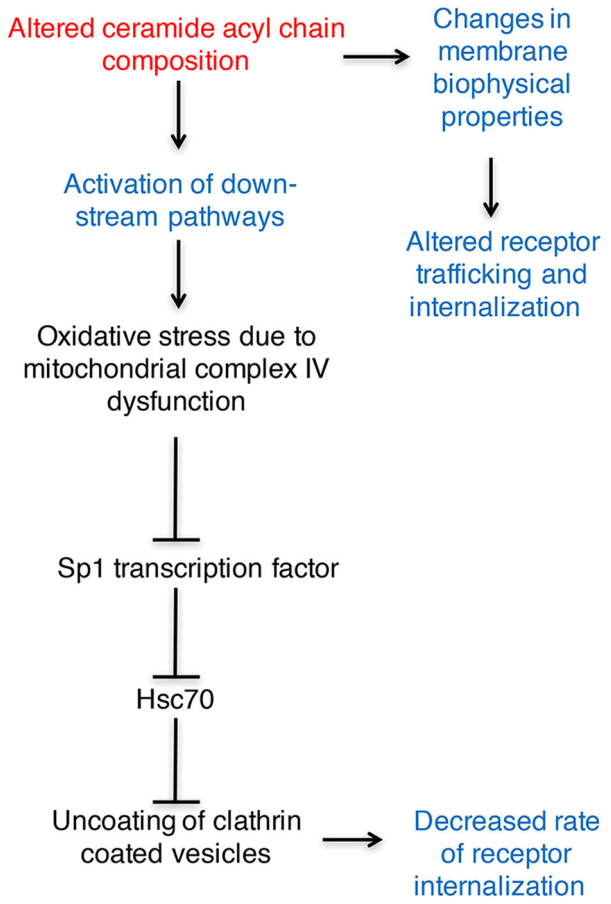

Fig. 7. Putative scheme of the effect of altering the SL acyl chain length on CME. Altering the SL acyl chain length (red) can either lead to changes in membrane biophysical properties or to activation of downstream pathways (blue). In the current study (black), we demonstrate the activation of one such pathway, which eventually leads to a reduced rate of CME.

Chromatin immunoprecipitation

ChIP was performed as described previously (Tarcic et al., 2016). Cells were fixed in 0.1 volume of formaldehyde (11% stock solution) followed by 0.06 volumes of 2.5 M glycine. Immunoprecipitation was performed using 3 µg of antibody in 0.1% Brij-35 solution. DNA was purified using a Qiagen PCR purification kit (Qiagen) followed by qPCR.

Reactive oxygen species

ROS were measured using chloro-methyl 6-carboxy-2′,7′-dichlorodihydrofluorescein diacetate (cmH_2DCF-DA) (Invitrogen). WT and CerS2 null astrocytes were incubated with 100 µM cmH_2DCF-DA or PBS for 30 min at 37°C and then washed three times with PBS. Conversion of cmH_2DCF-DA to cmDCF was determined using an Eclipse iCyt flow cytometer equipped with 488 nm solid state air cooled lasers, with 25 mW on the flow cell and with standard filter set-up; cmDCF was measured in the green channel with an excitation of 488 nm and emission of 525±50 nm.

Mitochondrial complex IV activity

Activities of mitochondrial respiratory chain complex IV and citrate synthase, a mitochondrial marker, were determined in cell homogenates as previously described (Saada et al., 2004). Measurements were performed using a double-beam spectrophotometer (UVIKON 930, Secomam, France).

Confocal microscopy

Confocal microscopy was performed using an Olympus IX 81 FluoView 1000 microscope and a UPLSAPO 60× objective. Images were processed and analyzed using FV-1000 software (Olympus, Tokyo, Japan).

Acknowledgements

We thank Mrs Shiri Graff from the laboratory of Dr Assaf Vardi for help with the FACS analysis of ROS and Mr Vladimir Kiss for assistance with high-resolution fluorescence and confocal microscopy.

Competing interests

The authors declare no competing or financial interests.

Author contributions

G.V. designed and performed the experiments and wrote the manuscript. S.B.-D. performed the bioinformatics analyses for Hsc70 promoter analysis and helped with writing the manuscript. O.T. performed the ChIP assays. J.D. and A.H.M. carried out the ESI-MS/MS analyses of SLs, and A.S. assayed complex IV activity. Y.P.-J. generated CerS2 null mice, and A.H.F. supervised and funded the studies and wrote the manuscript.

Supplementary material

Supplementary information available online at
http://jcs.biologists.org/lookup/doi/10.1242/jcs.199968.supplemental

Funding

This work was supported by the Israel Science Foundation (1728/15) and by National Institutes of Health grant GM076217. Deposited in PMC for release after 12 months.

References

Ali, M., Fritsch, J., Zigdon, H., Pewzner-Jung, Y., Schütze, S. and Futerman, A. H. (2013). Altering the sphingolipid acyl chain composition prevents LPS/GLN-mediated hepatic failure in mice by disrupting TNFR1 internalization. *Cell Death Dis.* **4**, e929.

Archer, M. C. (2011). Role of sp transcription factors in the regulation of cancer cell metabolism. *Genes Cancer* **2**, 712-719.

Cartharius, K., Frech, K., Grote, K., Klocke, B., Haltmeier, M., Klingenhoff, A., Frisch, M., Bayerlein, M. and Werner, T. (2005). MatInspector and beyond: promoter analysis based on transcription factor binding sites. *Bioinformatics* **21**, 2933-2942.

Cheng, Z.-J., Singh, R. D., Sharma, D. K., Holicky, E. L., Hanada, K., Marks, D. L. and Pagano, R. E. (2006). Distinct mechanisms of clathrin-independent endocytosis have unique sphingolipid requirements. *Mol. Biol. Cell* **17**, 3197-3210.

Florin, L., Becker, K. A., Sapp, C., Lambert, C., Sirma, H., Müller, M., Streeck, R. E. and Sapp, M. (2004). Nuclear translocation of papillomavirus minor capsid protein L2 requires Hsc70. *J. Virol.* **78**, 5546-5553.

Ghosh, R. N., Gelman, D. L. and Maxfield, F. R. (1994). Quantification of low density lipoprotein and transferrin endocytic sorting HEp2 cells using confocal microscopy. *J. Cell. Sci.* **107**, 2177-2189.

Greene, L. E. and Eisenberg, E. (1990). Dissociation of clathrin from coated vesicles by the uncoating ATPase. *J. Biol. Chem.* **265**, 6682-6687.

Han, I. and Kudlow, J. E. (1997). Reduced O glycosylation of Sp1 is associated with increased proteasome susceptibility. *Mol. Cell. Biol.* **17**, 2550-2558.

Hirst, J., Sahlender, D. A., Li, S., Lubben, N. B., Borner, G. H. H. and Robinson, M. S. (2008). Auxilin depletion causes self-assembly of clathrin into membraneless cages in vivo. *Traffic* **9**, 1354-1371.

Hsin, I.-L., Sheu, G.-T., Chen, H.-H., Chiu, L.-Y., Wang, H.-D., Chan, H.-W., Hsu, C.-P. and Ko, J.-L. (2010). N-acetyl cysteine mitigates curcumin-mediated telomerase inhibition through rescuing of Sp1 reduction in A549 cells. *Mutat. Res.* **688**, 72-77.

Jiang, M. and Chen, G. (2009). Ca2+ regulation of dynamin-independent endocytosis in cortical astrocytes. *J. Neurosci.* **29**, 8063-8074.

Keyel, P. A., Mishra, S. K., Roth, R., Heuser, J. E., Watkins, S. C. and Traub, L. M. (2006). A single common portal for clathrin-mediated endocytosis of distinct cargo governed by cargo-selective adaptors. *Mol. Biol. Cell* **17**, 4300-4317.

Kim, S. Y., Kang, H. T., Han, J. A. and Park, S. C. (2012). The transcription factor Sp1 is responsible for aging-dependent altered nucleocytoplasmic trafficking. *Aging Cell* **11**, 1102-1109.

Lauwers, E., Goodchild, R. and Verstreken, P. (2016). Membrane lipids in presynaptic function and disease. *Neuron* **90**, 11-25.

Levy, M. and Futerman, A. H. (2010). Mammalian ceramide synthases. *IUBMB Life* **62**, 347-356.

Mayor, S. and Pagano, R. E. (2007). Pathways of clathrin-independent endocytosis. *Nat. Rev. Mol. Cell Biol.* **8**, 603-612.

Megias, L., Guerri, C., Fornas, E., Azorin, I., Bendala, E., Sancho-Tello, M., Durán, J. M., Tomás, M., Gomez-Lechon, M. J. and Renau-Piqueras, J. (2000). Endocytosis and transcytosis in growing astrocytes in primary culture. Possible implications in neural development. *Int. J. Dev. Biol.* **44**, 209-221.

Meyer, S. G. E., Wendt, A. E., Scherer, M., Liebisch, G., Kerkweg, U., Schmitz, G. and de Groot, H. (2012). Myriocin, an inhibitor of serine palmitoyl transferase, impairs the uptake of transferrin and low-density lipoprotein in mammalian cells. *Arch. Biochem. Biophys.* **526**, 60-68.

Morales, A., Lee, H., Goñi, F. M., Kolesnick, R. and Fernandez-Checa, J. C. (2007). Sphingolipids and cell death. *Apoptosis* **12**, 923-939.

Park, J.-W., Park, W.-J., Kuperman, Y., Boura-Halfon, S., Pewzner-Jung, Y. and Futerman, A. H. (2012). Ablation of very long acyl chain sphingolipids causes hepatic insulin resistance in mice due to altered detergent-resistant membranes. *Hepatology* **57**, 525-532.

Park, W.-J., Park, J.-W., Erez-Roman, R., Kogot-Levin, A., Bame, J. R., Tirosh, B., Saada, A., Merrill, A. H., Pewzner-Jung, Y. and Futerman, A. H. (2013). Protection of a ceramide synthase 2 null mouse from drug-induced liver injury: role of gap junction dysfunction and connexin 32 mislocalization. *J. Biol. Chem.* **288**, 30904-30916.

Park, W.-J., Park, J.-W., Merrill, A. H., Storch, J., Pewzner-Jung, Y. and Futerman, A. H. (2014). Hepatic fatty acid uptake is regulated by the sphingolipid acyl chain length. *Biochim. Biophys. Acta* **1841**, 1754-1766.

Parry, S. N., Ellis, N., Li, Z., Maitz, P. and Witting, P. K. (2008). Myoglobin induces oxidative stress and decreases endocytosis and monolayer permissiveness in cultured kidney epithelial cells without affecting viability. *Kidney Blood Press. Res.* **31**, 16-28.

Pewzner-Jung, Y., Brenner, O., Braun, S., Laviad, E. L., Ben-Dor, S., Feldmesser, E., Horn-Saban, S., Amann-Zalcenstein, D., Raanan, C., Berkutzki, T. et al. (2010a). A critical role for ceramide synthase 2 in liver homeostasis: II. insights into molecular changes leading to hepatopathy. *J. Biol. Chem.* **285**, 10911-10923.

Pewzner-Jung, Y., Park, H., Laviad, E. L., Silva, L. C., Lahiri, S., Stiban, J., Erez-Roman, R., Brügger, B., Sachsenheimer, T., Wieland, F. et al. (2010b). A critical role for ceramide synthase 2 in liver homeostasis: I. alterations in lipid metabolic pathways. *J. Biol. Chem.* **285**, 10902-10910.

Pinto, S. N., Fernandes, F., Fedorov, A., Futerman, A. H., Silva, L. C. and Prieto, M. (2013). A combined fluorescence spectroscopy, confocal and 2-photon microscopy approach to re-evaluate the properties of sphingolipid domains. *Biochim. Biophys. Acta* **1828**, 2099-2110.

Poumay, Y. and Ronveaux-Dupal, M.-F. (1988). Incubation of endothelial cells in a superoxide-generating system: impaired low-density lipoprotein receptor-mediated endocytosis. *J. Cell. Physiol.* **136**, 289-296.

Riebeling, C., Allegood, J. C., Wang, E., Merrill, A. H. and Futerman, A. H. (2003). Two mammalian longevity assurance gene (LAG1) family members, trh1 and trh4, regulate dihydroceramide synthesis using different fatty acyl-CoA donors. *J. Biol. Chem.* **278**, 43452-43459.

Saada, A., Bar-Meir, M., Belaiche, C., Miller, C. and Elpeleg, O. (2004). Evaluation of enzymatic assays and compounds affecting ATP production in mitochondrial respiratory chain complex I deficiency. *Anal. Biochem.* **335**, 66-72.

Schildge, S., Bohrer, C., Beck, K. and Schachtrup, C. (2013). Isolation and culture of mouse cortical astrocytes. *J. Vis. Exp.* e50079.

Shakor, A. B. A., Taniguchi, M., Kitatani, K., Hashimoto, M., Asano, S., Hayashi, A., Nomura, K., Bielawski, J., Bielawska, A., Watanabe, K. et al. (2011). Sphingomyelin synthase 1-generated sphingomyelin plays an important role in transferrin trafficking and cell proliferation. *J. Biol. Chem.* **286**, 36053-36062.

Shaner, R. L., Allegood, J. C., Park, H., Wang, E., Kelly, S., Haynes, C. A., Sullards, M. C. and Merrill, A. H. (2009). Quantitative analysis of sphingolipids for lipidomics using triple quadrupole and quadrupole linear ion trap mass spectrometers. *J. Lipid Res.* **50**, 1692-1707.

Silva, L. C., Ben David, O., Pewzner-Jung, Y., Laviad, E. L., Stiban, J., Bandyopadhyay, S., Merrill, A. H., Prieto, M. and Futerman, A. H. (2012). Ablation of ceramide synthase 2 strongly affects biophysical properties of membranes. *J. Lipid Res.* **53**, 430-436.

Simons, K. and van Meer, G. (1988). Lipid sorting in epithelial cells. *Biochemistry* **27**, 6197-6202.

Singh, R. D., Marks, D. L. and Pagano, R. E. (2007). Using fluorescent sphingolipid analogs to study intracellular lipid trafficking. *Curr. Protoc. Cell Biol.* Chapter 24, Unit 24.1–24.1.19.

Sullards, M. C., Liu, Y., Chen, Y. and Merrill, A. H. (2011). Analysis of mammalian sphingolipids by liquid chromatography tandem mass spectrometry (LC-MS/MS) and tissue imaging mass spectrometry (TIMS). *Biochim. Biophys. Acta* **1811**, 838-853.

Tarcic, O., Pateras, I. S., Cooks, T., Shema, E., Kanterman, J., Ashkenazi, H., Boocholez, H., Hubert, A., Rotkopf, R., Baniyash, M. et al. (2016). RNF20 links histone H2B ubiquitylation with inflammation and inflammation-associated cancer. *Cell Rep.* **14**, 1462-1476.

Tidhar, R., Sims, K., Rosenfeld-Gur, E., Shaw, W. and Futerman, A. H. (2014). A rapid ceramide synthase activity using NBD-sphinganine and solid phase extraction. *J. Lipid Res.* **56**, 193-199.

Vitner, E. B., Farfel-Becker, T., Ferreira, N. S., Leshkowitz, D., Sharma, P., Lang, K. S. and Futerman, A. H. (2016). Induction of the type I interferon response in neurological forms of Gaucher disease. *J. Neuroinflamm.* **13**, 104.

Wilke, N., Sganga, M. W., Gayer, G. G., Hsieh, K. P. and Miles, M. F. (2000). Characterization of promoter elements mediating ethanol regulation of hsc70 gene transcription. *J. Pharmacol. Exp. Ther.* **292**, 173-180.

Yasuhara, K., Ohno, Y., Kojima, A., Uehara, K., Beppu, M., Sugiura, T., Fujimoto, M., Nakai, A., Ohira, Y., Yoshioka, T. et al. (2011). Absence of heat shock transcription factor 1 retards the regrowth of atrophied soleus muscle in mice. *J. Appl. Physiol.* **111**, 1142-1149.

Yim, Y.-I., Sun, T., Wu, L.-G., Raimondi, A., De Camilli, P., Eisenberg, E. and Greene, L. E. (2010). Endocytosis and clathrin-uncoating defects at synapses of auxilin knockout mice. *Proc. Natl. Acad. Sci. USA* **107**, 4412-4417.

Yu, A., Shibata, Y., Shah, B., Calamini, B., Lo, D. C. and Morimoto, R. I. (2014). Protein aggregation can inhibit clathrin-mediated endocytosis by chaperone competition. *Proc. Natl. Acad. Sci. USA* **111**, E1481-E1490.

Zhang, Y., Li, X., Becker, K. A. and Gulbins, E. (2009). Ceramide-enriched membrane domains–structure and function. *Biochim. Biophys. Acta* **1788**, 178-183.

Zigdon, H., Kogot-Levin, A., Park, J.-W., Goldschmidt, R., Kelly, S., Merrill, A. H., Scherz, A., Pewzner-Jung, Y., Saada, A. and Futerman, A. H. (2013). Ablation of ceramide synthase 2 causes chronic oxidative stress due to disruption of the mitochondrial respiratory chain. *J. Biol. Chem.* **288**, 4947-4956.

Zigdon, H., Savidor, A., Levin, Y., Meshcheriakova, A., Schiffmann, R. and Futerman, A. H. (2015). Identification of a biomarker in cerebrospinal fluid for neuronopathic forms of Gaucher disease. *PLoS ONE* **10**, e0120194.

Zou, X., Gao, Y., Ruvolo, V. R., Gardner, T. L., Ruvolo, P. P. and Brown, R. E. (2011). Human glycolipid transfer protein gene (GLTP) expression is regulated by Sp1 and Sp3: involvement of the bioactive sphingolipid ceramide. *J. Biol. Chem.* **286**, 1301-1311.

Table S1. Primers used in the current study

Gene	Primers
CerS1	TaqMan™(Mm00433562_m1)
CerS2	TaqMan™(Mm00504086_m1)
CerS3	TaqMan™(Mm03990709_m1)
CerS4	TaqMan™(Mm01212479_m1)
CerS5	TaqMan™(Mm00510996_g1)
CerS6	TaqMan™(Mm00556165_m1)
HPRT	TaqMan™(Mm00446968_m1)
Auxilin-1 (dnaj6C)	TaqMan™(Mm01265598_m1)
Hsc70	F: 5′-CTGCTGCTATTGCTTACGGC-3′
	R: 5′-TCAAAAGTGCCACCTCCCAA-3′
Fatty acid synthase	F: 5′-CAAGTGTCCACCAACAAGCG-3′
	R: 5′-GGAGCGCAGGATAGACTCAC-3′
Glycolipid transfer protein	F: 5′-CTGCCGCCCTTCTTTGATTG-3′
	R: 5′-AGGGTCTTGAACTTGGCTGG-3′
GFAP	F: 5′-TAGTCCAACCCGTTCCTCCA-3′
	R: 5′-CCAGTTGTCGACTAGGACCG-3′
Toll like receptor 4	F: 5′-ACCTGGCTGGTTTACACGTC-3′
	R: 5′-CTGCCAGAGACATTGCAGAA-3′
TBP	F: 5′-TGCTGTTGGTGATTGTTGGT-3′
	R: 5′-CTGGCTTGTGTGGGAAAGAT-3′
Hsc70 ChIP −68	F: 5′-ACCTAGGCGAGCGTTCTG-3′
	R: 5′-ACGACGAGACCACACAAATG-3′
Hsc70 ChIP −174	F: 5′-CCGAACGCTGCTCTCATTG-3′
	R: 5′-AACGCTCGCCTAGGTCCC-3′
Sp1	F: 5′-AATTTGCCTGCCCTGAGTGC-3′
	F: 5′-TTGGACCCATGCTACCTTGC-3′

F, forward; R, reverse.